Long-Term Behaviour of Norway Spruce Glulam Loaded Perpendicular to Grain

Francesco Mirko Massaro [1*], *Kjell Arne Malo* [1**]

[1] Department of Structural Engineering, Norwegian University of Science and Technology (NTNU), Rich. Birkelandsvei 1A, 7491, Trondheim, Norway

[*] corresponding author, francesco.m.massaro@ntnu.no , +4773413058

[**] kjell.malo@ntnu.no

ABSTRACT

The mechanical behaviour of timber loaded in compression perpendicular to grain is essential for a rational design of many timber structures. Structural components frequently exposed to such loading include studs on bottom rails, stress-laminated timber decks, timber elements lying in between vertical load-bearing columns as well as traditional timber joints mating surfaces in compression. Compression perpendicular to grain has been a repeated topic for discussion both in the current European regulations for timber structures, as well as in the ongoing work with the next generation of Eurocode 5 - timber structures. However, the long-term behaviour is quite complex, taking both time and moisture variation into consideration, and to improve the understanding and the ability to consider the long-term effects in practical design, a simplified one-dimensional model is given herein. The paper presents novel results from long-term compression orthogonal to grain tests performed with load and moisture control. The purpose of the testing was to evaluate the effect of transversal creep on the long-term behaviour of timber elements including the effect of the mechanosorptive deformation. The test results were in turn used to calibrate a one-dimensional model for the prediction of the long-term response of timber. The model takes into account the combined effects of loading and moisture variations. The effective material properties are defined by use of effective pith locations together with the orthotropic material parameters. Finally, a comparison between the model results and experimental observations is given, showing an overall good prediction of the response.

Keywords

glued-laminated timber, long-term behaviour, compression perpendicular to grain, creep, mechanosorption

1. INTRODUCTION

The mechanical response of timber changes with time when loaded. Moreover, the climate conditions of the surroundings have a significant influence on timber behaviour (Bodig and Jayne 1993). The dependency of the duration of the load and the climate conditions on the long term behaviour of timber has previously been studied and described for the longitudinal direction of the wood fibres (Mohager and Toratti 1993; Schniewind 1968; Toratti 1992). Ranta-Maunus (1993) showed the importance of creep in the direction perpendicular to grain. Furthermore, several studies have been performed with focus on the orthogonal direction showing the influence of the moisture content variation on the dimensional stability and moisture induced stresses of timber cross-sections (Bengtsson 1999; Svensson and Toratti 2002). Additionally, several authors addressed the phenomenon of the non-linearity of the creep deformation (Hunt 1989; Morlier and Palka 1994; Reichel and Kaliske 2015). Ozyhar, Hering and Niemz (2013) have performed several tests, including compression perpendicular to grain tests, to study the viscoelastic behaviour of wood loaded for 24 hours.

The main objective of the present study is to quantify proper material parameters to describe the long-term behaviour of timber under compression orthogonal to grain and exposed to moisture variation. Additionally, the determined viscoelastic and moisture related properties are used to develop a one-dimensional model to describe the orthogonal to grain behaviour of timber. The model is suitable for evaluation of long-term compressive loading perpendicular to the grain if the distribution of stresses can approximately be treated as a one-dimensional case, and there is no need of evaluating the full stress distribution, using more computationally heavy 3D models (Massaro and Malo 2017). Examples on such structural cases popular in timber engineering are pre-stressed timber decks used in road bridges, header joist, or more generally floors, beams, and deck plates lying in between vertical load-bearing structures, which conservatively can be treated as one-dimensional.

In order to achieve these objectives, an experimental study on orthogonally compressed timber is performed in order to obtain the required data for the simulations. The one-dimensional model, implemented and used in this study, is based on the viscoelastic-mechanosorptive model suggested by Toratti (1992). To evaluate properly the mechanosorptive effect, a proper moisture diffusion analysis is required (Muszyński et al. 2005). Hence, the moisture content of timber is evaluated according to the moisture-transport model proposed by Fortino, Mirianon and Toratti (2009). The implementation of the model is explained in detail. Finally, the calculated results from the simulations are compared with the measured values of the creep experiments.

2. MATERIALS AND METHODS

2.1 TEST SETUP

The present investigation has been motivated by the need for more accurate models for the long-term behaviour of pre-stressed timber decks. This type of decks on road bridges is often made out of parallel side-by-side glulam beams mechanically held together by pre-stressed steel rods, installed in pre-drilled holes in the perpendicular direction relative to the grain. The pre-stressing rods are usually located in the central part of the beam. The compressive stress together with the friction between the beams forms a two-dimensional decking plate (Fig. 1) (Dahl et al. 2006; Ekholm 2013; Pousette et al. 2002; Pousette et al. 2017; Ritter 1992).

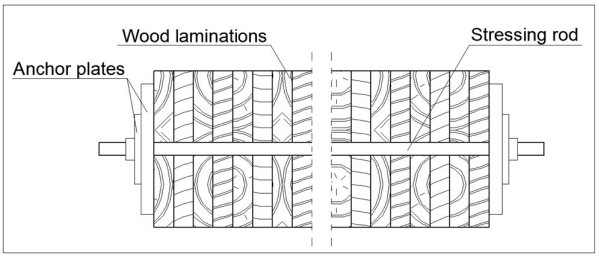

Fig. 1 Section of a pre-stressed timber bridge deck (after Ritter (1992))

The long-term compression tests were performed on specimens of Norway spruce classified as GL30c according to NS-EN 14080:2013. The specimens were obtained by cutting a timber beam (GL30c) with cross-section of 360×115 mm^2. Firstly, the four outermost lamellae were cut and removed in order to get specimens made only by the four inner lamellae, consider Fig. 2. The reason for the removal of the external lamellae was that timber class GL30c, as all the classes ending with the letter “c”, has outer lamellae with different properties than the inner ones. The pre-stressing rods are usually located in the inner lamellae. Therefore, there was the need to remove the outer lamellae in order to obtain data valid for the softer central part of the beams, and to perform the tests on lamellae with the

same classification. Afterwards, the inner lamellae were sliced every 100 mm along the longitudinal direction, giving cuboids of dimension 100×115×180 mm^3 (Fig. 2). A hole of 22 mm diameter was drilled in the centre of the minor faces of the cuboids to allow for insertion of a load-transferring rod.

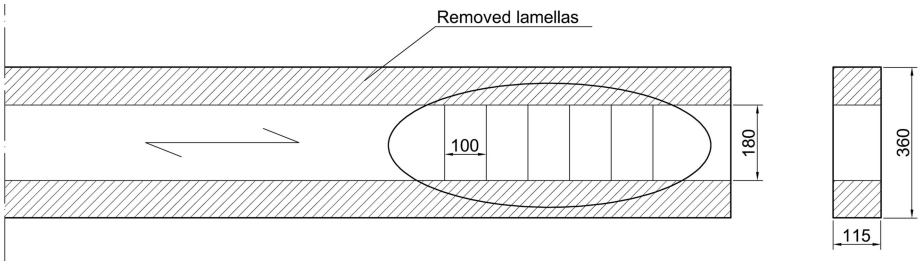

Fig. 2 Location of the cuboidal specimens in a glulam beam (units in mm)

All specimens were made of a stack of five cuboids of dimension 100×115×180 mm^3. Each cuboid had a hole of 22 mm diameter in the centre of its top face. The total length of the specimen stack was 900 mm and the cross-section 100×115 mm^2 (Fig. 3a).

A rod of 16mm diameter was inserted into the hole to hold the cuboids together and to load the specimens (Fig. 3b). The direction of the rod was orthogonal to the direction of the wood fibres, in order to compress it in the orthogonal direction.

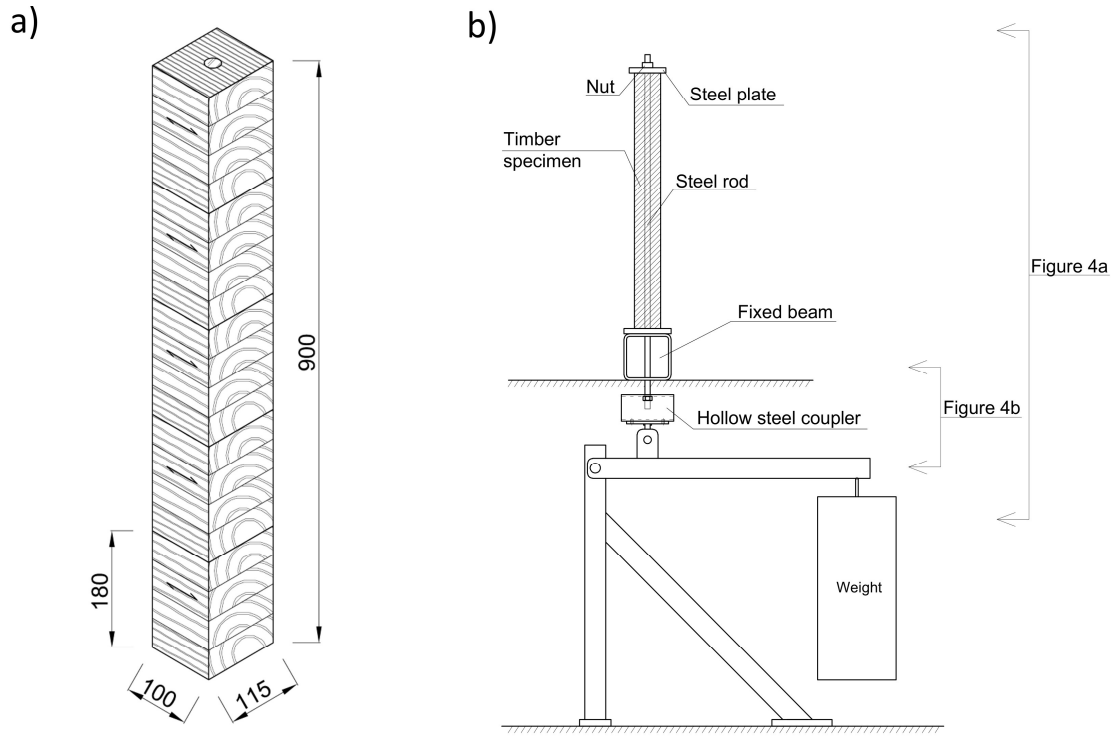

Fig. 3 a) Sketch of a timber specimen (units in mm); b) lateral view of the test setup

The principle of the experimental setup is shown in Fig. 3b and photos are given in Fig. 4a and Fig. 4b. The setup consists of a small steel structure comprising a lever arm in order to impose gravity loading on the specimens.

The specimens were loaded through steel rods, which transfer the forces from the lever arms, passing the hollow steel coupler also through holes, and finally coupled to steel plates on top of the specimens, inducing compression on the wooden blocks.

The dimensional changes of the specimens were measured by displacement transducers (LVDT with accuracy higher than 0.03 mm) located on the outside of the hollow steel coupler, shown in Fig. 3b and Fig. 4b. These transducers sampled the change in distance between the hollow steel coupler and the fixed beam which, by subtracting the elastic elongation of the rods, corresponds to the vertical dimensional change of the timber specimens (Fig. 4b).

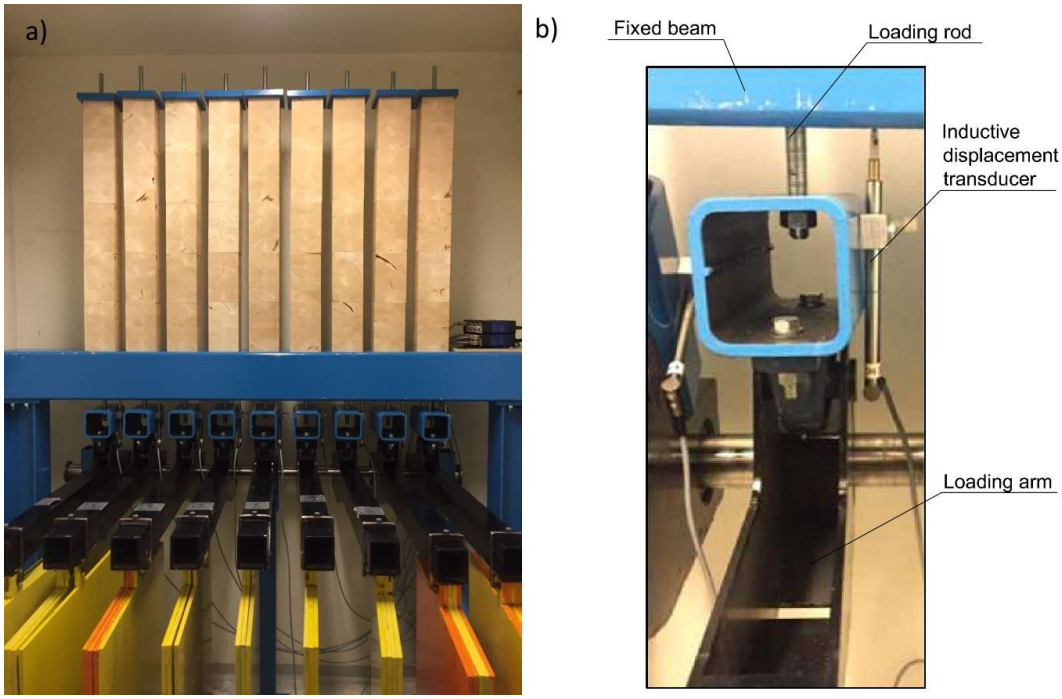

Fig. 4 a) Detail of the experimental rig showing the 9 timber specimens and the 9 lever arms loaded with different number of steel plates; b) Detail of a measuring transducer (LVDT) showing the hollow steel coupler between the loading rod and the lever arm

2.2 TEST METHOD

The tests were performed in a climate-controlled room with constant temperature of 20 °C and continuous control of the relative humidity in the air. Prior to testing, the specimens were conditioned to a temperature of 20 °C and a relative humidity of 65% for several weeks. In the first phase of testing, which lasted 4 months, the nine specimens were tested in parallel maintaining the relative humidity (RH) constant at the value of 65% in order to evaluate the viscoelastic effects without the influence of the variation of the moisture content in wood. In the second phase, the test continued with a variation of relative humidity between 80% and 50% in order to evaluate the mechanosorptive effects in the specimens.

The specimens were tested under three different load conditions, which correspond to a uniform perpendicular compression stress on the timber of 0.6, 0.8 and 1 MPa, respectively. The corresponding force, assuming that the

whole load is transferred to the timber, was checked by use of a load-cell prior to testing. The three values of compression stress were chosen in order to replicate the stress levels of interest in real structures such as stress-laminated decks.

2.3 ONE-DIMENSIONAL MODEL

The experiments are modelled by a simplified one-dimensional model in order to evaluate the viscoelastic and the mechanosorptive parameters. The geometry of the specimens is modelled by a one-dimensional line, 900mm long, fixed at the bottom and free at the top vertex (Fig. 5a).

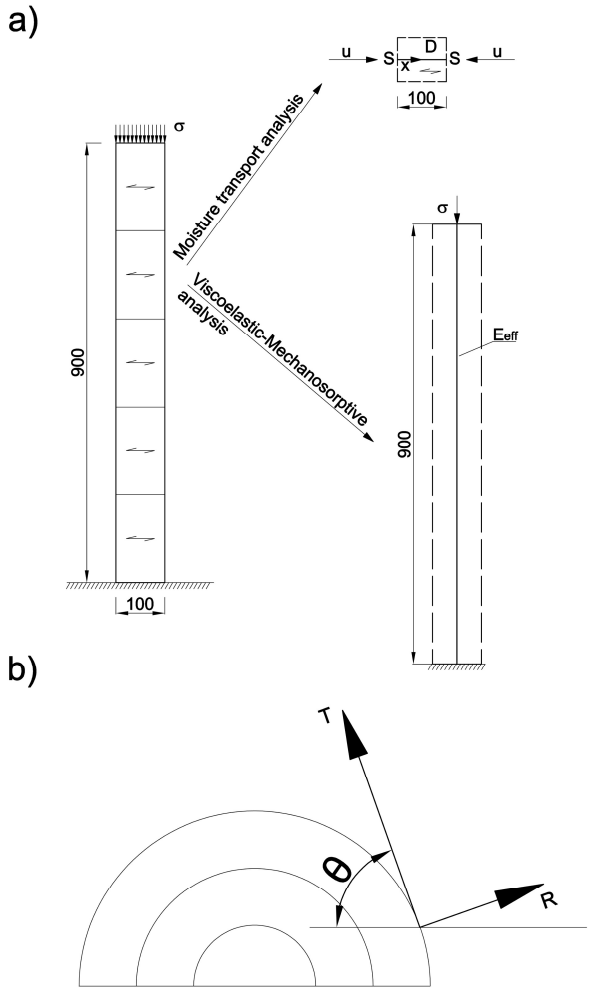

Fig. 5 a) Schematic representation of a specimen and of the one-dimensional approaches used for the models; b) angle between the tangent to the annual ring at a given point and the horizontal axis

2.3.1 MOISTURE TRANSPORT MODEL

It is assumed that the moisture transport in the timber follows Fick's second law of diffusion. Since all the vertical faces of the specimens are exposed to the air, it is assumed that the diffusion of moisture is dominated by the longitudinal to grain direction (x-direction: Fig. 5a). Therefore, Fick's law for calculation of the moisture content u in the timber specimens is simplified as shown in Equation (1).

$$\frac{\partial u}{\partial t} = \frac{\partial}{\partial x}\left(D\frac{\partial u}{\partial x}\right) \tag{1}$$

The diffusion coefficient D is dependent on the moisture content and in this analysis the values obtained by Sjödin (2006) for Norway Spruce in the longitudinal to grain direction are used. From a mathematical point of view, the moisture diffusion, Equation (1), is similar to the heat transfer Equation (2), where ρ is the density of timber, c_T is the specific heat, T is temperature and λ is the conductivity.

$$\rho c_T \frac{\partial T}{\partial t} = \frac{\partial}{\partial x}\left(\lambda\frac{\partial T}{\partial x}\right) \tag{2}$$

The equivalence is obtained considering $T = u$, $\lambda = \rho\, D$ and $c_T = 1$ (Fortino et al. 2009).

Due to this analogy, the diffusion analysis was performed with the aid of the software Comsol Multiphysics (COMSOL Inc. 2017) using the physics of heat transfer.

The moisture flux across the boundary is produced by the difference between the moisture content at the surface of timber u_{surf} and the equilibrium moisture content of timber for the current relative humidity of the air u_{eq}.

$$\left(D\frac{\partial u}{\partial x}\right) = S(u_{eq} - u_{surf}) \tag{3}$$

In Equation (3) the surface emission factor S is considered equal to $10\ x\ 10^{-8}$ m s^{-1} (Angst and Malo 2013).

The equilibrium moisture content u_{eq} is calculated by Equation (4) according to Avramidis (1989), where the temperature T is expressed in Kelvin and RH is the relative humidity of the air.

$$u_{eq} = 0.01\left[\frac{-T\ln(1-RH)}{0.13\left(1-\frac{T}{647.1}\right)^{-6.46}}\right]^{\frac{1}{110T^{-0.75}}} \tag{4}$$

In order to perform the analysis by the software Comsol Multiphysics, the geometry of the specimens was simplified to a 1D element in the x-direction, see Fig. 5a, considering only diffusion of moisture in the longitudinal to grain direction. The diffusion perpendicular to grain direction is neglected since the diffusion coefficient in this direction belongs to a smaller order of magnitude (Sjödin 2006).

The moisture content values, obtained through the moisture transport analyses performed with the software Comsol Multiphysics, are then averaged over the width in order to be used in the mechanical model described in Chapter 2.3.2.

2.3.2 VISCOELASTIC-MECHANOSORPTIVE MODEL

The model used for the analysis is proposed by Toratti (1992) and expresses the total strain rate $\dot{\varepsilon}$ as the sum of the elastic strain rate $\dot{\varepsilon}_e$, the shrinkage-swelling strain rate $\dot{\varepsilon}_s$, the viscoelastic creep strain rate $\dot{\varepsilon}_v$ and the mechanosorptive strain rate $\dot{\varepsilon}_{ms}$, as given by Equation (5).

$$\dot{\varepsilon} = \dot{\varepsilon}_e + \dot{\varepsilon}_s + \dot{\varepsilon}_v + \dot{\varepsilon}_{ms} \tag{5}$$

The presence of the holes in the specimen is accounted using the net timber area. Otherwise, it is neglected since the area of the holes is only 3% of the net timber area. The time-dependent deformation of the steel rod for these levels of stress and temperature is negligible (Anderberg 1988; Schneider and Lange 2011).

Elastic deformation

The elastic deformation ε_e is provided by Hooke's law, Equation (6), where E_{eff} is the effective modulus of elasticity calculated by Equation (7). Here, the mechanical properties in radial and tangential directions are transformed to an average effective direction according to Häglund (Häglund 2010) in order to relate 1D models to orthotropic material properties. The same approach is used for the other parameters described in Equations (11), (17) and (18), as shown by Angst and Malo (2010).

$$\sigma = E_{eff}\ \varepsilon_e \tag{6}$$

$$E_{eff} = \frac{E_R E_T G_{RT}}{E_T G_{RT} c^2 (c^2 - s^2 \nu_{RT}) + E_R G_{RT} s^2 (s^2 - c^2 \nu_{TR}) + E_R E_T s^2 c^2} \tag{7}$$

In Equation (7), E_R and E_T are the modulus of elasticity in the radial and in the tangential direction respectively, G_{RT} is the rolling shear modulus, ν_{RT} and ν_{TR} are the Poisson ratios about the radial and the tangential directions, s=sin θ and c=cos θ, where θ is the angle between the tangent to the annual ring at a given point and the horizontal axis, see illustration in Fig. 5b.

The mechanical properties in the transversal direction used in the model were chosen after an optimization process. Numerical simulations of the geometry of the specimens, which includes the pith locations of the laminations, were performed with the software Abaqus (Dassault Systemes 2014). The Abaqus model includes the geometry of the specimens loaded elastically by a uniform compression load. The coordinates of all pith locations are given in Appendix B (Online Resource). The Abaqus model is then given as input for the optimization in the software Isight (Dassault Systemes 2017). The software Isight optimized the simulations, using the Pointer algorithm, varying the transversal mechanical properties (E_T, E_R, G_{RT}, ν_{RT}) in order to obtain an elastic vertical displacement in the numerical models coinciding with the experimental results. The measured elastic vertical displacement is also equal to $\sigma \cdot {}^{L}/_{E_{eff,exp}}$, where L is the specimen length (900 mm). The optimization showed the existence of several sets of properties which would lead approximately to the same displacement. The elastic properties proposed by Dahl (Dahl 2009; Dahl and Malo 2009) (Table 1) resulted as one of the possible sets of properties obtained from the Isight optimization and therefore they have been selected to be used in this study.

The representative angle θ for each specimen was also obtained through numerical simulation of the geometry of the specimens with the software Abaqus. These simulations were performed using the mechanical properties (E_R, E_T, G_{RT}, ν_{RT}) in Table 1. The numerically obtained E_{eff} and the mechanical properties given in Table 1 were inserted into Equation (7) and therefore the representative angle θ for each specimen was calculated. However, the dependency between θ and E_{eff} is represented through a non-injective function, so the angles chosen are the highest between the two mathematically possible solutions and they are also given in Table 2.

The "real" effective moduli of elasticity of the specimens at the beginning of the test ($E_{eff,exp}$) were obtained experimentally from the measured elastic strains. They are shown in Table 2, where Latin capitals indicate specimen identification, while the following number gives the stress level in MPa.

Table 1 Timber properties used in the model: reference values (Dahl 2009; Dahl and Malo 2009)

E_T	E_R	G_{RT}	ν_{RT}
[MPa]	[MPa]	[MPa]	[-]
352	818	31	0.835

Table 2 Values of the representative angle between rings and horizontal axis (θ), of the effective numerical modulus of elasticity ($E_{eff,num}$) and of the effective experimental modulus of elasticity ($E_{eff,exp}$)

Specimen	A-1.0	B-1.0	C-1.0	A-0.8	B-0.8	C-0.8	A-0.6	B-0.6	C-0.6
θ [deg]	78.13	76.90	76.90	77.48	77.00	77.33	77.29	78.04	77.37
$E_{eff,num}$ [MPa]	260.9	248.0	248.0	254.0	249.0	252.4	252.1	260.0	252.9
$E_{eff,exp}$ [MPa]	255.7	238.9	247.7	229.3	229.8	259.8	224.8	266.5	238.8

The rate form of Equation (6), given in Equation (8), takes also the variation of the effective modulus into account caused by the change of moisture content (MC).

$$\dot{\varepsilon}_e = \dot{E}_{eff}^{-1}\sigma + E_{eff}^{-1}\dot{\sigma} \tag{8}$$

The dependence on MC of the moduli of elasticity, both normal and shear, can be expressed as in Equation (9), according to (Santaoja et al. 1991). The reference values of the moduli refer to a moisture content of 12%.

$$E_i = E_{i,ref}\left[1 - 2.6\left(u - u_{ref}\right)\right] \qquad G_{RT} = G_{RT,ref}\left[1 - 2.6\left(u - u_{ref}\right)\right]$$
$$i\text{=R,T} \qquad u_{ref} = 0.12 \tag{9}$$

Hygroscopic deformation

The hygroscopic strain rate $\dot{\varepsilon_s}$ is modelled proportional to the rate of moisture content $\dot{u}$ as shown in Equation (10).

$$\dot{\varepsilon}_s = \alpha_{eff}\,\dot{u} \tag{10}$$

$$\alpha_{eff} = \alpha_R c^2 + \alpha_T s^2 \tag{11}$$

In Equation (11), α_R and α_T are the hygro-expansion coefficients for the radial and the tangential direction, respectively.

Viscoelastic creep deformation

The viscoelastic creep deformation ε_v is the component of the total deformation solely dependent on time.

$$\varepsilon_v = \Phi(t) \cdot \varepsilon_e \tag{12}$$

In Equation (12), Φ is the creep function (Dinwoodie 2000).

For computational reasons, the creep functions Φ obtained from the empirical creep data have been fitted into series of Kelvin bodies, Equation (13).

$$\Phi = \sum_n S_n \left(1 - e^{-\frac{t}{\tau_n}}\right) \tag{13}$$

Here, S_n represents the final compliance of the Kelvin element n relative to the elastic compliance and τ_n is the retardation time of the element n (Toratti 1992).

The use of series of Kelvin bodies is physically suitable to describe the creep phenomenon, since the physical behaviour of timber suggests that viscoelastic compressive deformation cannot increase unlimited but must tend to an asymptotic value.

Mechanosorptive deformation

The mechanosorptive deformation is the component of deformation due to the interaction of stress and moisture content variations.

Svensson and Toratti (2002) showed that the mechanosorptive strain ε_{ms} is the sum of a recoverable part $\varepsilon_{ms,r}$ and an irrecoverable part $\varepsilon_{ms,i}$ expressed in Equation (14).

$$\varepsilon_{ms} = \varepsilon_{ms,r} + \varepsilon_{ms,i} \tag{14}$$

The recoverable part is modelled by the creep limit model given by Equation (15), where S^{∞} is the compliance at the mechanosorptive creep limit, τ is the considered instant of time and m is a material parameter (Hunt and Shelton 1988; Toratti 1992).

$$\varepsilon_{ms,r} = S^{\infty}\sigma\left\{1 - e^{-m\int_0^{\tau}|du(t)|}\right\} \tag{15}$$

The irrecoverable mechanosorptive strain exists only in presence of moisture content never reached before by the loaded timber element.

$$\dot{\varepsilon}_{ms,i} = m_v\sigma\left|\dot{U}\right| \tag{16}$$

In Equation (16), m_v is a material parameter independent of moisture, and U is a moisture content value not previously reached during the load history of the material.

Defining the mechanosorptive compliance matrices as assumed by Fortino et al. (2009) (see Online Resource Appendix A.1.2), it is possible to apply the same approach as used for the evaluation of the effective elastic modulus of elasticity, in order to calculate the mechanosorptive compliance and the irrecoverable mechanosorptive parameter for the representative orientation of the 1D model.

$$S^{\infty} = \frac{E_T G_{RT} c^2(c^2 - s^2\nu_{RT}) + E_R G_{RT} s^2(s^2 - c^2\nu_{TR}) + E_R E_T s^2 c^2}{E_R G_{RT}} m_T \tag{17}$$

$$m_v = \frac{E_T G_{RT} c^2(c^2 - s^2\nu_{RT}) + E_R G_{RT} s^2(s^2 - c^2\nu_{TR}) + E_R E_T s^2 c^2}{E_R G_{RT}} m_{vT} \tag{18}$$

In Equations (17) and (18), m_T and m_{vT} represent respectively the mechanosorptive compliance and the irrecoverable mechanosorptive parameter in the tangential material direction. The full derivation of the equations is given in Online Resource Appendix A.1.2.

The value for the material parameter m, equal to 2.5, was chosen according to Toratti (1992).

2.4 INCREMENTAL MODEL

A detailed derivation of the expressions in the model is given in the Appendix (Online Resource). Here, only the resulting expressions are outlined.

Elastic and hygroscopic strain increment

The elastic strain increment $\Delta\varepsilon_e$ expressed in Equation (19) is easily obtained from Equation (8).

$$\Delta\varepsilon_e = \Delta E_{eff}^{-1}\sigma + E_{eff}^{-1}\Delta\sigma \tag{19}$$

The variation of the elastic compliance ΔE_{eff}^{-1} is due to the variation of moisture content as described in Equation (9).

The hygroscopic strain increment $\Delta\varepsilon_s$, given in Equation (20), is straightforwardly obtained from Equation (10).

$$\Delta\varepsilon_s = \alpha_{eff}\Delta u \tag{20}$$

Creep strain increment

The creep strain increment $\Delta\varepsilon_v$ is evaluated using Equations (12), (13) and the trapezoidal rule (Toratti 1992).

$$\Delta\varepsilon_v = E_{eff}^{-1}\sum_n S_n\left(1 - e^{-\frac{\Delta t}{\tau_n}}\right)\left(\sigma_{n,hist} + \frac{\Delta\sigma}{2}\right) \tag{21}$$

$$\sigma_{n.hist}^{t+1} = \left(\sigma_{n,hist} + \frac{\Delta\sigma}{2}\right)e^{-\frac{\Delta t}{\tau_n}} + \frac{\Delta\sigma}{2} \tag{22}$$

In Equation (21), the term $\sigma_{n,hist}$ represents the stress history values of each Kelvin body updated through the Equation (22).

Mechanosorptive strain increment

The mechanosorptive recoverable strain increment $\Delta\varepsilon_{ms,r}$ is evaluated by Equation (23), and it is calculated, similarly to the creep strain increment, by use of the trapezoidal rule (Toratti 1992). The stress history term $\sigma_{n,hist,m}$ is updated through Equation (24).

$$\Delta\varepsilon_{ms,r} = S^{\infty}\left(1 - e^{-m|\Delta u|}\right)\left(\sigma_{n,hist,m} + \frac{\Delta\sigma}{2}\right) \tag{23}$$

$$\sigma_{n.hist,m}^{t+1} = \left(\sigma_{n,hist,m} + \frac{\Delta\sigma}{2}\right)e^{-m|\Delta u|} + \frac{\Delta\sigma}{2} \tag{24}$$

The mechanosorptive irrecoverable strain $\Delta\varepsilon_{ms,i}$, Equation (25), is obtained directly from Equation (16).

$$\Delta\varepsilon_{ms,i} = m_v\sigma|\Delta U| \tag{25}$$

2.4.1 ALGORITHM FOR SIMULATION

The computations are performed according to the following algorithm for each time step:

- Evaluate the moisture content u using the software Comsol Multiphysics.
- Update the mechanical properties of timber according to the moisture content
- Compute the stress distribution
    - For $t = t_0 = 0$, it is considered elastic (Equation (6))
    - For $t > t_0$, it is considered, as a first attempt, equal to the previous increment, $\sigma^{(t=n)} = \sigma^{(t=n-1)}$, and thus $\Delta\sigma = 0$.

- Compute the strain increments $\Delta\varepsilon_e$, $\Delta\varepsilon_s$, $\Delta\varepsilon_v$, $\Delta\varepsilon_{ms,r}$, $\Delta\varepsilon_{ms,i}$ using Equations (19), (20), (21), (23) and (25), respectively.
- Check that the stress distribution is in equilibrium with the external load
    - If not, evaluate $\Delta\sigma$ and re-compute the strain increments (back to the previous point of the algorithm)
    - Iterate until $\left|(\Delta\sigma^{iter=i+1} - \Delta\sigma^{iter=})/\sigma\right| < 10^{-5}$
- Update $\sigma^{(n)} = \sigma^{(n-1)} + \Delta\sigma$, and all the strain components
- Update $\sigma_{n,hist}$ and $\sigma_{n,hist,m}$
- Add time increment and restart the algorithm

Note that in a creep analysis, the stress is constant during the whole analysis and therefore $\Delta\sigma$ is always equal to 0. This means that each step is performed without the need of internal iterations.

3. RESULTS AND DISCUSSION

3.1 EXPERIMENTAL RESULTS

3.1.1 TEST RESULTS UNDER CONSTANT CLIMATE CONDITIONS

For four months, the specimens were tested keeping constant both the temperature (20° C) and the relative humidity (65 %) of the surrounding air. Under these conditions, the wood deformations are only dependent on the stress and by the duration of it, due to the viscoelastic behaviour of timber. Since the load, and hence the stress, is constant during the whole experiment for each specimen, it is possible to evaluate the influence of the duration of the load on the deformations. For the first three hours, the data were collected every second, then every 10 seconds for a week. Afterwards, the data were collected every hour for the remaining duration of the experiment. The elastic elongation of the rod has been subtracted from the collected displacements in order to obtain the average strain related only to the timber specimen. The results in Fig. 6 show that the average strain increases in absolute value with the time, as expected.

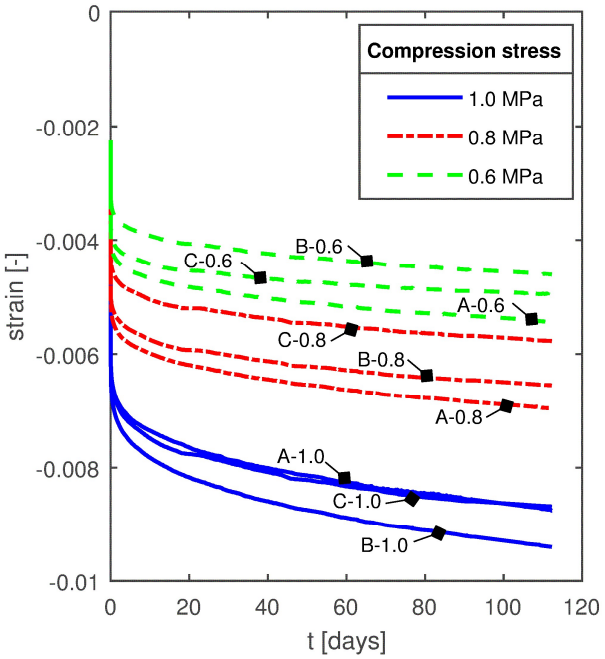

Fig. 6 Strain vs time behaviour of the 9 specimens under constant climate conditions

The fit of the empirical data to the series of Kelvin bodies, defined in Equation (13), was performed with the least squares method choosing the retardation time τ_n in a logarithmic scale. The data referring to the same stress level were simultaneously fitted to one set of Kelvin bodies. For each stress level, the fit was performed minimizing the error given by the sum of the three squared differences of the three curves of that specific stress level. Thus, the fit led to three sets of coefficients S_n, shown in Table 3, one for each set of specimens loaded by the same stress level.

Table 3 Final compliances of the element n relative to the elastic compliances S_n and their retardation time τ_n

	σ = 0.6 MPa	σ = 0.8 MPa	σ = 1 MPa
τ_n [days]	S_n [-]	S_n [-]	S_n [-]
0.1	0.535	0.459	0.552
1	0.106	0.087	0.129
10	0.116	0.129	0.168
100	0.303	0.317	0.419
1000	0.653	0.383	0.442
10000	0.173	0.451	0.512

Therefore, the three obtained functions, defined by the coefficients given in Table 3 and describing specimens with the same stress level, can be considered as optimized creep curves and are shown in Fig. 7. Note that the used measurements lasted about 115 days, thus the values for 1000 and 10000 days are extrapolated. However, the mathematical properties of Equation (13) assure that the curve is asymptotic.

The plot in Fig. 7 shows that the creep function can be treated independent of the stress level for stresses smaller than a certain limit. The linearity between stress and strain is achieved only for compression stress levels of 0.6 and 0.8 MPa. For the stress level of 1 MPa, the linearity with respect to stress is not followed and the creep function shows a higher level of strain. Therefore, above 30% to 40% of the characteristic strength the behaviour of timber probably starts to behave non-linear with respect to stress. The non-linear behaviour has also been described in

(Schniewind 1968) and (Toratti 1992) with regards to tension and bending. Local nonlinearities due to point loads or joints are not studied in this work.

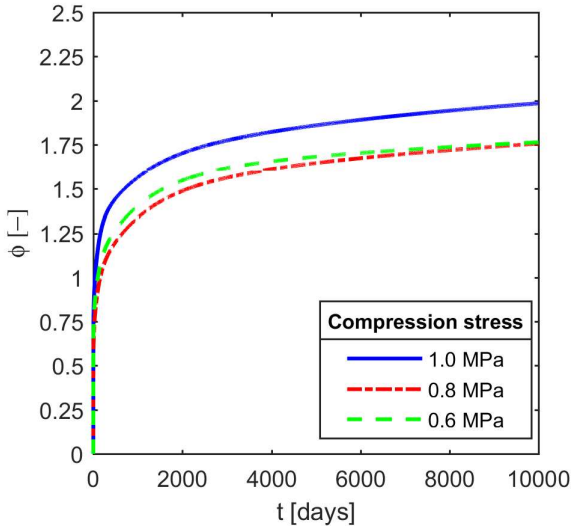

Fig. 7 Optimized creep curves for each stress level

3.1.2 TEST RESULTS UNDER VARIABLE RELATIVE HUMIDITY

After four months, the relative humidity was changed several times between the RH values of 80% and 50%, as shown in Fig. 8. The measured strains in the specimens during this time of exposure are plotted in Fig. 8.

Since the deformation of the specimens is assumed to be the sum of the elastic deformation, the viscoelastic creep deformation, the mechanosorptive deformation and the deformation due to the volumetric change, it was possible to evaluate the deformations related to the mechanosorptive effects.

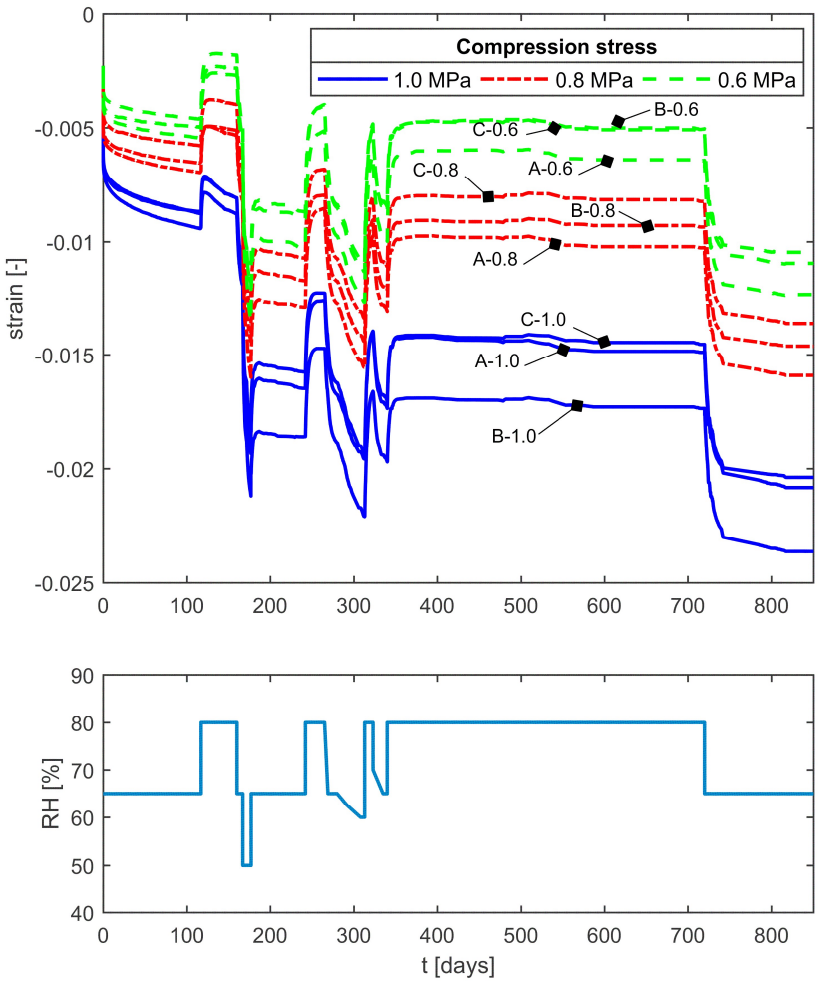

Fig. 8 Strain vs time behaviour of the 9 specimens under variable climate conditions

Subtracting the deformation caused by the volumetric change, comparisons of the strain rates of the timber specimens in the phases before and after the variations of RH could be made. It was noticed that the strain rate increased after every variation of the relative humidity in the room. Without any change of RH, the specimens would have deformed with a smaller strain rate but, due to the variation of RH, the strain rate became much higher and this effect increases with increasing stress level.

3.2 OPTIMIZATION OF THE PARAMETERS

The hygro-expansion coefficients were determined by fitting the experimental results of each specimen with the least squares optimization method. The fit gives optimal results when using different coefficients for the processes of wetting and drying, in accordance with Angst and Malo (2012). The ratios between the tangential and the radial values of the obtained coefficients are in good agreement with Dinwoodie (2000). The values of the hygro-expansion coefficients are given in Table 4.

The tangential mechanosorptive limit compliance m_T and the tangential irrecoverable mechanosorptive parameter m_{vT} were also obtained by fitting the experimental results using the least squares optimization method. The values which best fit the experimental results of each specimen were then averaged and are given in Table 4.

Table 4 Hygro-expansion coefficients and parameters used in the mechanosorptive constitutive equations

Wetting	Hygro-expansion coefficient in tangential direction	α_T	0.1541
	Hygro-expansion coefficient in radial direction	α_R	0.0847
Drying	Hygro-expansion coefficient in tangential direction	α_T	0.1341
	Hygro-expansion coefficient in radial direction	α_R	0.0736
Tangential mechanosorptive limit compliance		m_T	0.0096 MPa^{-1}
Tangential irrecoverable mechanosorptive parameter		m_{vT}	0.0757 MPa^{-1}

3.3 DISCUSSION OF THE MODEL RESULTS

There have been performed simulations of the nine experiments presented in Chapter 2. The model explained in Chapter 2.3 and Chapter 2.4 has been implemented in the software Matlab (MathWorks 2017), except for the moisture transport model which is implemented in the software Comsol Multiphysics. The results from the moisture transport analyses are then given as input in Matlab. The elastic properties used in the simulations are described in Table 1, the viscoelastic parameters in Table 3, and the mechano-sorptive parameters in Table 4.

The results obtained from the simulations show good overall agreement with the experimental results depicted in Fig. 8. Comparisons between the model and the experimental results for each stress level are plotted in Fig. 9.

The simulations also show different curves for each specimen even if the compression stress is the same. This is due to the use of different values of the effective material properties in each analysis by the introduction of an average pith location (Table 2) in the model by use of a representative angle between the tangent to the annual rings and the horizontal direction.

The simulations show somewhat less accuracy in case of rapid humidity variation, but the overall trend is respected and the resulting differences in values between model and experimental strains remain small, as shown in Fig. 9. In general, the results show that the present model, described in the previous chapters, performs very well with regard to the long-term behaviour of timber subjected to uniform cross-grain compression and varying climate conditions.

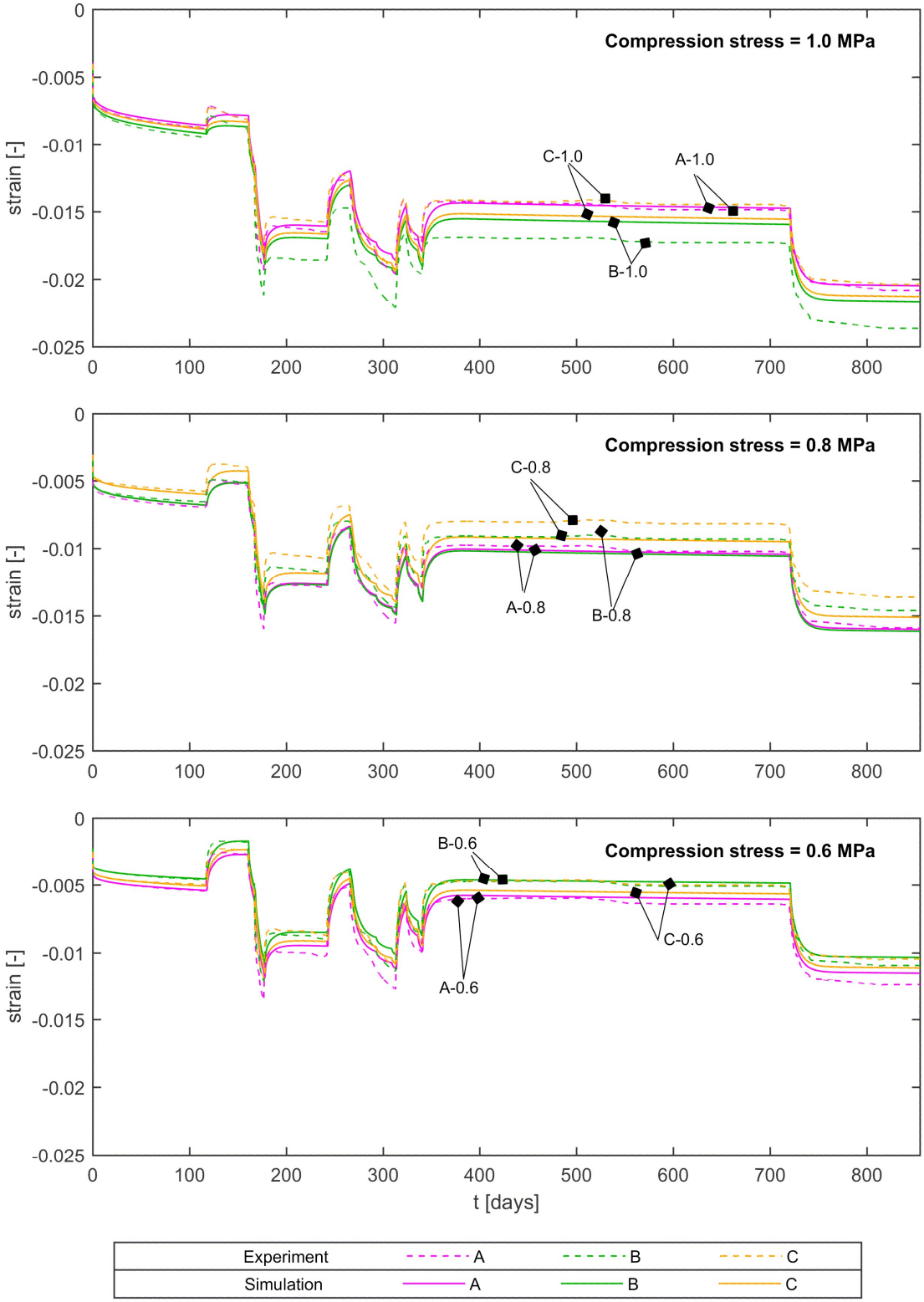

Fig. 9 Comparison between model and experimental results

4. CONCLUSION

The objective of this study was to investigate the long-term behaviour of glulam of Norway Spruce in the direction perpendicular to the grain and to calibrate a simple one-dimensional model for the description of the deformations in this direction.

The examination of the results of the performed experiments under constant relative humidity showed a non-linear dependency of the strain with respect to the stress.

The set of model parameters calibrated in this study or retrieved from previous studies describe well the phase with variable relative humidity and gave an overall good agreement between experimental results and simulations from the implemented one-dimensional model.

In addition, the study showed the importance of the proper material modelling, herein by use of effective pith locations, as shown also by Angst and Malo (2012), in order to properly represent the material properties in a simplified 1D model, and thereby describe the deformations with good accuracy. However, a sensitivity analysis for further study is suggested.

For prediction of cases which cannot be modelled as a one-dimensional problem, it is necessary to expand the study using a three-dimensional approach in order to evaluate the relations between the longitudinal and the perpendicular to grain behaviour.

ACKNOWLEDGMENTS

This work was funded by the WoodWisdom-Net+ project DuraTB ("Durable Timber Bridges") and the support from the funding bodies and partners is gratefully acknowledged.

Conflict of interest

On behalf of all authors, the corresponding author states that there is no conflict of interest.

REFERENCES

Anderberg Y (1988) Modelling Steel Behaviour. Fire Saf J 13:17-26

Angst V, Malo KA (2010) Moisture induced stresses perpendicular to the grain in glulam: review and evaluation of the relative importance of models and parameters. Holzforschung 64:609-617

Angst V, Malo KA (2012) The effect of climate variations on glulam—an experimental study. Eur J Wood Wood Prod 70:603-613

Angst V, Malo KA (2013) Moisture-induced stresses in glulam cross sections during wetting exposures. Wood Sci Technol 47:227-241

Avramidis S (1989) Evaluation of "three-variable" models for the prediction of equilibrium moisture content in wood. Wood Sci Technol 23:251-257

Bengtsson C (1999) Mechano-sorptive creep in wood - experimental studies of the influence of material properties. Dissertation, Chalmers University of Technology

Bodig J, Jayne BA (1993) Mechanics of Wood and Wood Composites. Krieger Publishing Company,

COMSOL Inc. (2017) COMSOL Multiphysics 5.3.

Dahl KB (2009) Mechanical properties of clear wood from Norway spruce. Doctoral dissertation, Norwegian University of Science and Technology

Dahl KB, Bovim NI, Malo KA (2006) Evaluation of Stress Laminated Bridge Decks Based on Full Scale Tests. Paper presented at the 9th World Conference on Timber Engineering, Portland, OR, USA,

Dahl KB, Malo KA (2009) Linear shear properties of spruce softwood. Wood Sci Technol 43:499-525 doi:10.1007/s00226-009-0246-5

Dassault Systemes (2014) Abaqus/CAE 6.14.

Dassault Systemes (2017) Isight.
Dinwoodie JM (2000) Timber: Its Nature and Behaviour. 2nd edn. E & FN Spon - Taylor & Francis, London & New York
Ekholm K (2013) Performance of Stress-Laminated Timber Bridge Decks. Doctoral dissertation, Chalmers University of Technology
Fortino S, Mirianon F, Toratti T (2009) A 3D moisture-stress FEM analysis for time dependent problems in timber structures. Mech Time-Depend Mater 13:333-356
Häglund M (2010) Parameter influence on moisture induced eigen-stresses in timber. Eur J Wood Wood Prod 68:397-406
Hunt DG (1989) Linearity and non-linearity in mechano-sorptive creep of softwood in compression and bending. Wood Sci Technol 23:323-333 doi:10.1007/bf00353248
Hunt DG, Shelton CF (1988) Longitudinal moisture-shrinkage coefficients of softwood at the mechano-sorptive creep limit. Wood Sci Technol 22:199-210
Massaro FM, Malo KA (2017) Anchor plates for pre-stressing rods and compression orthogonal to grain of timber. Paper presented at the 3rd International Conference on Timber Bridges - ICTB 2017, Skellefteå, Sweden, 26-29 June 2017
MathWorks (2017) MATLAB vol R2017a.
Mohager S, Toratti T (1993) Long term bending creep of wood in cyclic relative humidity. Wood Sci Technol 27:49-59 doi:10.1007/bf00203409
Morlier P, Palka LC (1994) Basic knowledge. In: Morlier P (ed) RILEM Report 8 - Creep in Timber Structures. E & FN Spon, London, pp 9-42
Muszyński L, Lagaňa R, Shaler SM, Davids WG (2005) Comments on the experimental methodology for determination of the hygro-mechanical properties of wood. Holzforschung 59:232-239
Ozyhar T, Hering S, Niemz P (2013) Viscoelastic characterization of wood: Time dependence of the orthotropic compliance in tension and compression. Journal of Rheology 57:699-717 doi:10.1122/1.4790170
Pousette A, Jacobsson P, Gustafsson M, Horttanainen J, Dahl K (2002) Stress Laminated Bridge Decks, Part II. Trätek, Skellefteå
Pousette A, Massaro FM, Malo KA, Fortino S, Salokangas L, Wacker J (2017) Wooden bridge decks. In: Pousette A, Malo KA, Thelandersson S, Fortino S, Salokangas L, Wacker J (eds) Durable Timber Bridges - Final Report and Guidelines (SP Rapport). RISE Research Institute of Sweden, Skellefteå, pp 111-132
Ranta-Maunus A (1993) Rheological behaviour of wood in directions perpendicular to the grain. Mater Struct 26:362-369
Reichel S, Kaliske M (2015) Hygro-mehcanically coupled modelling of creep in wooden structures, Part I: Mechanics. Internation Journal of Solids and Structures 77:45-64 doi:https://doi.org/10.1016/j.ijsolstr.2015.07.019
Ritter MA (1992) Timber bridges: design, construction, inspection, and maintenance. U.S. Department of Agriculture, Forest Service, Washington DC
Santaoja K, Leino T, Ranta-Maunus A, Hanhijärvi A (1991) Mechano-sorptive Structural Analysis of Wood by the ABAQUS Finite Element Program vol 1276. VTT Technical Research Centre of Finland - Research Notes. VTT, Espoo
Schneider R, Lange J (2011) Constitutive Equations and Empirical Creep Law of Structural Steel S460 at High Temperatures. Journal of Structural Fire Engineering 2:217-230
Schniewind AP (1968) Recent progress in the study of the rheology of wood. Wood Sci Technol 2:188-206 doi:10.1007/BF00350908
Sjödin J (2006) Steel-to-timber dowel joints: Influence of moisture induced stresses. Doctoral Dissertation, Vaxjo University
Svensson S, Toratti T (2002) Mechanical response of wood perpendicular to grain when subjected to changes of humidity. Wood Sci Technol 36:145-156 doi:10.1007/s00226-001-0130-4
Toratti T (1992) Creep of timber beams in a variable environment. Doctoral Dissertation, Helsinki University of Technology